47th AIAA Aerospace Sciences Meeting Including The New Horizons Forum and Aerospace Exposition
5 - 8 January 2009, Orlando, Florida

AIAA 2009-1136

A Hybrid WENO Scheme for Simulation of Shock Wave-Boundary Layer Interaction

Maher Lagha [*], Xiaolin Zhong, Jeff Eldredge, John Kim

Mechanical and Aerospace Engineering Department, University of California, Los Angeles

420 Westwood Plaza, Los Angeles CA 90095-1597, USA

The ultimate goal of this study is to develop a robust and accurate numerical method for simulation of hypersonic turbulent boundary layers. A hybrid numerical method, coupling a fifth-order weighted essentially non-oscillatory (WENO) scheme for shock capturing and a centered fourth-order finite difference scheme for computing turbulence away from the shock, is considered. It is applied, in this paper, to a benchmark problem in which shock-shock and shock-vortex interactions are present. It is shown that this method captures the shocks robustly and computes the flow away from the shocks accurately. Then, a spatially evolving turbulent boundary layer at Mach number 2.5 is considered. The issue of turbulent inflow generation, using rescaling/recycling method, is addressed.

I. Introduction

A critical issue in computational hypersonic aerodynamics is to find a robust and accurate way of calculating shock-boundary layer interactions. Toward this end, several numerical techniques for shock capturing have been developed over the past several decades. Examples include, but not limited to, the shock capturing total variation diminishing (TVD) schemes (e.g. Daru & Tenaud (2001)[1]) and WENO schemes (e.g. Shu & Osher (1989),[2] Jiang & Shu (1996)[3]).

TVD schemes are suitable for simulations of supersonic flows with a small number of isolated shock waves. However, near the shocks, the accuracy is reduced to first-order and solutions are degraded by excessive numerical diffusion. Thus, problems involving multiple shocks and a large number of complex flow structures away from shocks would require a more accurate numerical scheme.

WENO schemes have been proven to be efficient in some benchmark test cases, where the one-dimensional Euler equation is considered. However, due to the way the Euler flux is evaluated, this scheme is computationally expensive and it is highly dissipative. Variants of WENO schemes, which are more suitable for simulation of compressible turbulent flows, have been developed (e.g. Weirs & Candler (1997)[4] and Martn *et al.* (2006)[5]). By modifying the standard strategy of computing the weights of the stencils in the WENO scheme,[3] Wang & Chen (2001)[6] developed an optimized WENO scheme, by which short waves (waves with wavelength of $\approx 6\ dx$, where dx is the grid spacing) can be resolved better. However, their optimized scheme was not tested in a benchmark problem relevant to simulation of compressible turbulent flows.

Conventional finite-difference schemes, high-order ones in particular, are more appropriate for accurately resolving short waves. However, they are not suitable for flows with shock waves since they induce large oscillations near discontinuities.

Hybrid approaches, which use a WENO scheme near discontinuities and a less dissipative and more efficient finite-difference scheme away from discontinuities, have been proposed. In general, a hybrid scheme is computationally more efficient since it limits the expensive flux evaluation of a WENO scheme near discontinuities only.

Adams & Shariff (1996),[7] who used an essentially non oscillatory (ENO) scheme coupled with a compact finite-difference scheme, were among the first to use a hybrid method. Their hybrid scheme was quite successful in computing the interaction of a shock wave and divergence-free vortices. Adams[8,9] used the same hybrid methodology for simulation of a supersonic turbulent boundary layer along a compression

[*]maher@seas.ucla.edu

ramp. Pirozolli (2002)[10] improved Adams & Shariff's[7] method by replacing the ENO scheme with a WENO scheme.

Ren *et al.*(2003)[11] demonstrated that a sharp transition from one scheme to the other could cause spurious oscillations, which could be avoided or minimized by using a weighted average of both schemes. Kim & Kwon (2005)[12] extended the work of Ren *et al.* by coupling the WENO scheme with a 6th-order central difference scheme. By splitting the WENO scheme into two parts, a central flux part and a numerical dissipation part, their scheme can be seen as a 6th-order central finite difference scheme, where its shock capturing ability is guaranteed by adding a numerical dissipation, adaptively controlled by the weighting function. They used the same weighting function as that used by Ren *et al.* Kim & Kwon's scheme was better in terms of computing time and resolution: it was nearly twice faster than the method by Ren *et al.* (the slowness of the compact scheme of Ren *et al.* is due to the inversion of the tridiagonal matrix).

In spite of the much effort aimed at improving hybrid methods for simulation of aerodynamic problems, there has been relatively few studies aiming at testing and improving hybrid methods for viscous boundary-layer problems. The objective of the present work is to examine the capability of hybrid methods in simulating complex viscous flows, involving the interaction between a shock wave and boundary layer. The ultimate goal of our work is to develop a robust and accurate numerical method that can be used for simulation of hypersonic turbulent boundary layers, where we have to accurately capture shocks and complex turbulence structures.

II. A Benchmark Test Problem

The shock wave-boundary layer interaction is an important phenomena of supersonic and hypersonic flows. It is observed in many internal and external flow problems relevant to hypersonic space vehicles. Maximum fluctuating pressure levels and thermal loads, to which a structure is exposed, are generally found in regions of shock-boundary layer interactions, and they can affect the structural integrity of the vehicle.[13] Despite a remarkable progress in computational capabilities, some flow features are still predicted with large uncertainty (e.g. temperature peaks in strong interactions), and, more fundamentally, the fundamental physical processes of turbulent hypersonic boundary layers are still not well understood.

As a first step to test our numerical method in handling shock-boundary layer interactions, we investigated the reflection of a shock wave at the end wall of a shock tube. This is the same test problem considered by Weber *et al.* (1995),[14] who used a flux-corrected transport algorithm (FCT). Daru & Tenaud (2001)[1] obtained better results by using a high resolution TVD scheme with a new family of limiters. They also suggested that other approaches, such as a WENO scheme, would do a better job. Sjogreen & Yee (2003)[16] compared a WENO scheme with an improved TVD scheme, leading to results similar to those of Daru & Tenaud. Neither of these investigators used a hybrid method. Our objective is to evaluate a hybrid numerical method for capturing the shock and for computing the complicated shock-shock and shock-vortex interactions in a viscous boundary layer as well as for computing smooth parts of the flow.

III. Hybrid WENO Schemes

We solved the compressible Navier-Stokes equations written in non-dimensional form as given in Daru & Tenaud.[1] No slip boundary conditions were used at the adiabatic walls of a 2-D box $x \in [0,1] \times y \in [0,1]$, filled initially with an ideal gas at rest and separated at $x = 0.5$ by a membrane with a shock Mach number equal to 2.37. The dimensionless initial states are:[1]

$$\rho = 120, p = 120/\gamma, \text{ for } x \leq 0.5,$$

$$\rho = 1.2, p = 1.2/\gamma, \text{ for } x \geq 0.5,$$

where ρ, p and $\gamma = 1.4$ denote, respectively, density, pressure and the constant specific heat ratio. The Prandtl number is 0.73 and the considered Reynolds number is 200. Following Daru & Tenaud,[1] the viscosity is assumed to be constant and independent of the temperature.

We use a 4th-order central difference scheme for evaluating the spatial derivatives in the viscous fluxes as follows. For simplification, we consider only one spatial dimension. First, we denote the N_x discretisation points by x_i, where i=1,2,..N_x-2 for the interior points and i=0 or i=$N_x - 1$ for the boundary points.

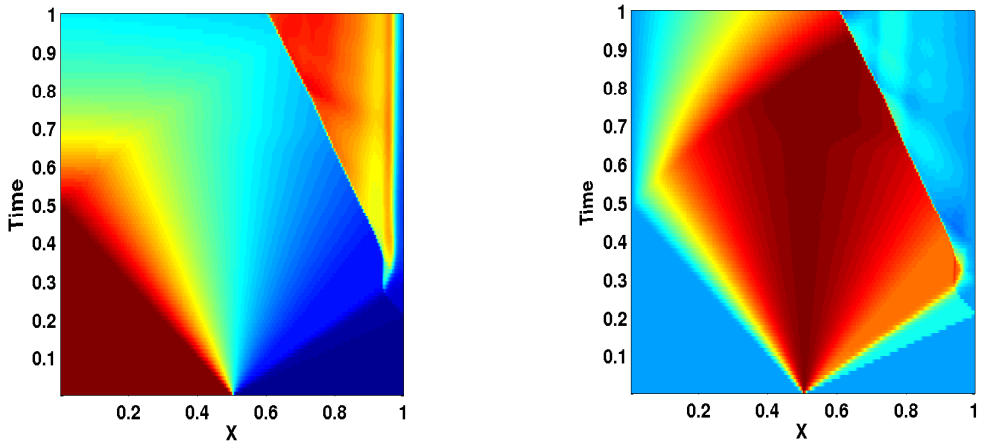

Figure 1. Spatio-temporal evolution of the density (left) and the streamwise momentum (right) along the centerline y=0.5. The shock is reflected at $t \approx 0.2$. Results at $t = 1$ are considered in the text.

Then, we have for any function $f = f(x)$ represented in discrete form as f_i=$f(x_i)$, the following 4th-order scheme:

$$\begin{aligned}
\left.\frac{\partial f}{\partial x}\right|_{\mathrm{i}} &= \frac{1}{12dx}(8(f_{i+1}-f_{i-1})-(f_{i+2}-f_{i-2})), \quad i=2,..N_{\mathrm{x}}-3,\\
\left.\frac{\partial f}{\partial x}\right|_{0} &= \frac{1}{6dx}(18(f_1-f_0)-9(f_2-f_0)+2(f_3-f_0)),\\
\left.\frac{\partial f}{\partial x}\right|_{1} &= \frac{1}{6dx}(2(f_1-f_0)+6(f_2-f_1)-(f_3-f_1)),\\
\left.\frac{\partial f}{\partial x}\right|_{\mathrm{N_x}-2} &= \frac{1}{6dx}(2(f_{N_{\mathrm{x}}-1}-f_{N_{\mathrm{x}}-2})+6(f_{N_{\mathrm{x}}-2}-f_{N_{\mathrm{x}}-3})-(f_{N_{\mathrm{x}}-2}-f_{N_{\mathrm{x}}-4})),\\
\left.\frac{\partial f}{\partial x}\right|_{\mathrm{N_x}-1} &= \frac{1}{6dx}(18(f_{N_{\mathrm{x}}-1}-f_{N_{\mathrm{x}}-2})-9(f_{N_{\mathrm{x}}-1}-f_{N_{\mathrm{x}}-2})+2(f_{N_{\mathrm{x}}-1}-f_{N_{\mathrm{x}}-4})),
\end{aligned}$$

where dx is the spatial step ($dx = 1/(N_{\mathrm{x}}-1)$).
Around the shocks, the Euler fluxes are computed using a 5th-order WENO decomposition/reconstruction.[2] For the evaluation of these Euler fluxes, a characteristic-based approach is applied, which uses the Roe-type approximate Riemann solver. We also consider the global Lax-Friedrichs flux, which is less time consuming than the former method and simpler to implement. For the time marching we use the standard 4th-order Runge-Kutta algorithm. The CFL number is set to 0.1 for all the considered resolutions mentioned below.

Like other hybrid methods, the choice of using one scheme instead of the other for a given cell, is based on the smoothness property of the solution. This smoothness can be measured, for example, by its gradients as used by Adams & Shariff ([7]). In the present work, we have used the smoothness indicator used by Ren *et al.*:[11]

$$r_{j+1/2} = \min(\mathrm{r_j}, \mathrm{r_{j+1}})$$

where

$$r_j = \frac{2\Delta f_{j+1/2}\Delta f_{j-1/2}+\epsilon}{(\Delta f_{j+1/2})^2+(\Delta f_{j-1/2})^2+\epsilon}.$$

The ϵ is a positive real number and Δ denotes the standard difference operator. Above a certain threshold r_{thres}, the solution is considered as non-smooth and the WENO scheme has to be applied. Although we use the same smoothness indicator as Ren *et al.* and Kim & Kwon, we do not use an average of both sub-schemes in each computational cell. Only one sub-scheme is used, the WENO or the finite-difference scheme. Hence our method is expected to be faster than the previous methods.

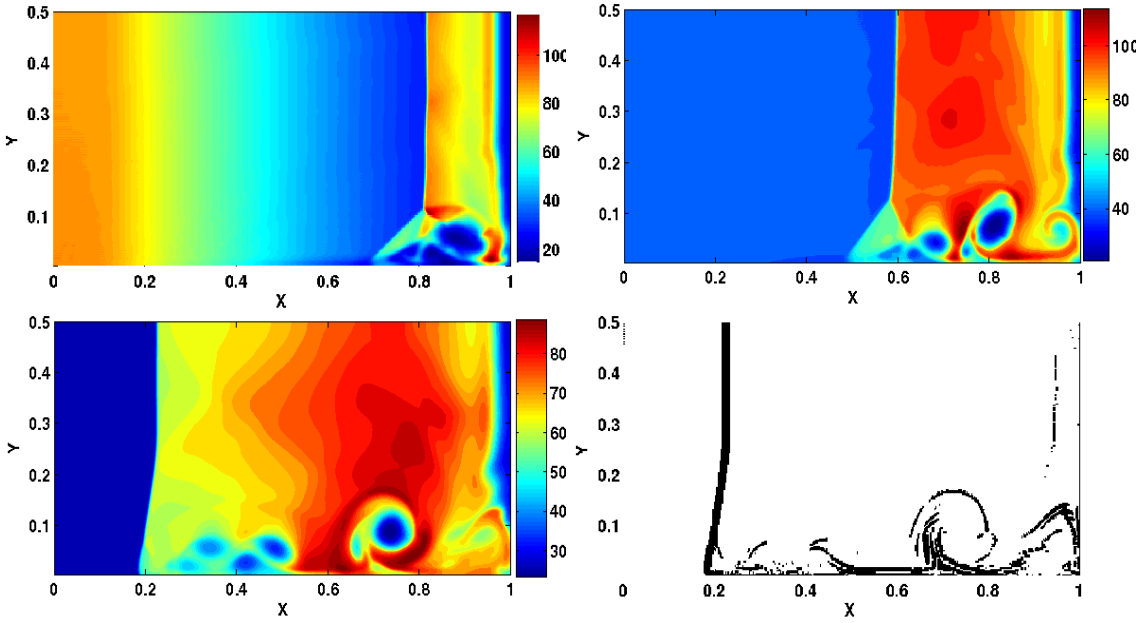

Figure 2. Temporal evolution of the density at time t=0.6. (top-left), t=1 (top-right) and t=1.4 (bottom-left). The points where the WENO scheme is applied are depicted by black points (bottom-right).

The performance of a smoothness indicator relies on its dependency on the threshold chosen by the user. If this threshold is too high, the WENO scheme might not be used in some points of discontinuity, which are interpreted as smooth points. This will ultimately lead to numerical instabilities. In contrast, if the threshold is too low, the WENO scheme would be used in smooth regions, thus increasing the computational cost of the hybrid method. The quality of the solution will be degraded due to the extra numerical dissipation introduced by the WENO scheme. The choice of the threshold value, which is mainly based on trial and errors, would be simplified if the value returned by the smoothness indicator is bounded. This is the case since from the definition above, we have $r_{j+1/2} \in [0; 1]$.

IV. Numerical Results

The temporal evolution of the flow can be illustrated by one of its velocity components or by its density. Following the numerical results in the literature, this evolution will be presented using the density and the streamwise velocity. Their spatio-temporal evolutions are given in Fig. 1, while the spatial distribution of the density is shown in Fig. 2 at three different instances. The resolution used in this figure is $(N_x \times N_y)$=(400×400), where N_x and N_y denote the number of points in the x- and y-direction respectively. Because the solution is symmetric with respect to the centerline y=0.5, only the half domain is shown.

First, a left-going expansion wave and right-going shock wave and a contact discontinuity are generated (Fig. 1). A boundary layer is formed near the top and bottom walls behind the right traveling wave. After t=0.2, the shock is reflected and a complex shock wave-boundary-layer interaction takes place. On one hand, the bifurcated foot from the shock ($x \approx 0.5$, t=1) and tail shock ($x \approx 0.6$, t=1) merge with the main reflected shock at a triple point, resulting in a λ-shape shock pattern. A separated flow region "bubble" appears when the static pressure behind the reflected shock is larger than the stagnation pressure in the boundary layer in reflected shock fixed coordinates. On the other hand, after the passage of the shock, a shear layer is formed with the triple point as its origin. It is unstable and rolls up to form discrete vortices at a later time (for time $t \geq$0.6). A detailed discussion of the flow structure near the λ-shape pattern is presented, for example, in Weber[14] or Davies & Wilson.[15]

In Figure 2, the points where the WENO scheme is used are shown with black points. In these points, the solution was flagged as non smooth. We see that the shock is well captured by the hybrid method. Some regions around the vortices are also considered as non-smooth. It is clear that this is related to the choice of

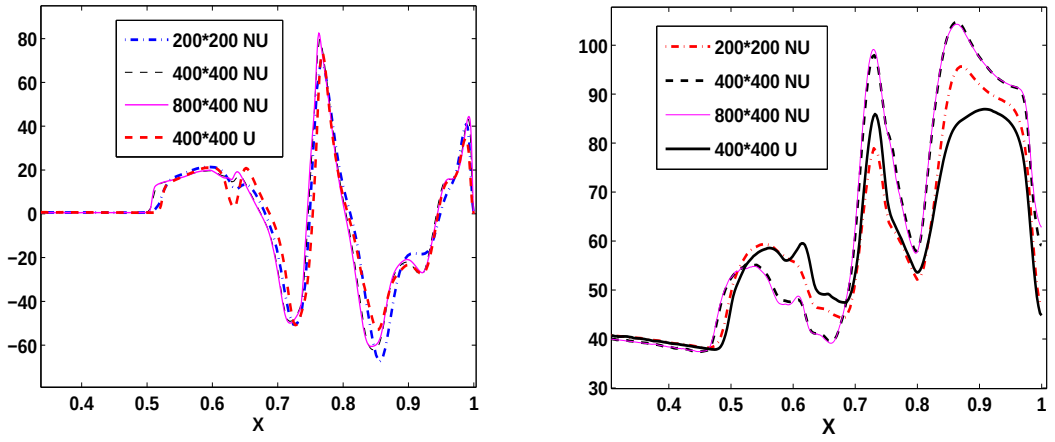

Figure 3. Distribution of the y-momentum ρv along the horizontal line y=0.05 (left) and the density ρ along the bottom wall (right) using different resolutions ($N_x \times N_y$) with the non-uniform meshes (denoted by NU) and a uniform mesh (denoted by U).

the threshold in the smoothness indicator, that is defined by the user. Therefore, it is natural to check the independence of the solution with respect to this threshold. We have checked that by decreasing r_{thres} from r_{thres}=10^{-1} to r_{thres}=10^{-2}, the WENO scheme is applied in additional points which have been considered smooth before. The solution however remains almost the same, especially the locations of the shock and of the vortices.

In order to better resolve near-wall structures, we also used a non-uniform mesh (ξ, η) clustered near the walls using the following hyperbolic tangent function with β=1.2:

$$y = \frac{1}{2}\left(1 + \frac{\tanh(\beta(2\xi - 1))}{\tanh(\beta)}\right)$$

where $y \in [0, 1]$ and $\xi \in [0, 1]$ is the new coordinate. The same clustering is used in the other direction x.

Using this non-uniform mesh, three resolutions have been considered: (200×200), (400×400) and (800×400). The last two resolutions are quite similar and hence the resolution (400×400) can be considered a reference solution for this study. All the structures, especially the vortices on the right of the reflected shocks, are well resolved.

For a more quantitative result, the distribution of the density along the bottom wall is shown in Fig. 3. There are two peaks of density near the vortices. The magnitude of these picks depends on the resolution, and it appears to be converged with the high resolution (400×400) using the non-uniform mesh, since its distributions for (400×400) and (800×400) are indistinguishable. Regarding the vortices, the convergence of the method can be attested for by considering the distribution of the y-momentum ρv along the horizontal line corresponding to y=0.05. First, the upwelling ($\rho v \geq 0$) and downwelling ($\rho v \leq 0$) motions associated with these vortices can be easily identified from Fig. 3. Second, the magnitude of these peaks are almost the same for high resolutions, from (400×400) to (800×400). Therefore, the solution has already converged with a non-uniform resolution (400×400), which is lower than those used by Daru & Tenaud[1] (uniform mesh with 3000×1500) .

Finally, it is worthy to examine the influence of the flux-splitting method. Figure 4 shows the density distribution obtained with both flux-splitting methods mentioned above. The resolution used in both cases is (400×400), and we used the same CFL number. From a qualitative point of view, these solutions are similar. The solution obtained with the characteristic scheme introduces some noise, whereas it is smoothed out with the more dissipative global Lax-Friedrichs scheme. We have remarked that at low resolution, the characteristic scheme with the Roe average produces negative density on the right of the reflected shock. This might be related to the main drawback of the standard Roe's approximate Riemann solver in dealing with high speed flow near low density regions.[17] But in our case, it provides good results with higher resolution.

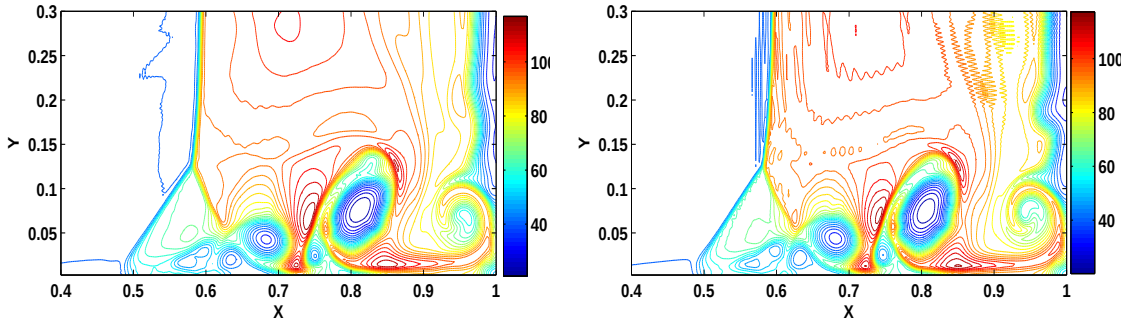

Figure 4. The density contours at t=1 using two different flux types. Left: Lax-Friedrichs splitting. Right: characteristic decomposition using Roe average.

V. Hypersonic Boundary Layer

The ultimate objective of our study is to investigate the fundamental physics of turbulence in hypersonic boundary layers. In this section we report preliminary results obtained from a simulation of a spatially developing turbulent boundary layer at a relatively low Mach number as a validation of our numerical method described above as well as other numerical procedures in simulating spatially developing turbulent boundary layers.

A. The governing equations

The compressible Navier-Stokes equations in conservative form are non-dimensionalized with the free-stream quantities (ρ_∞, T_∞, U_∞, μ_∞). The lengths are non-dimensionalized using the boundary-layer thickness at the inlet δ^i_{99} and the time by δ^i_{99}/U_∞. The ratio of specific heats, γ, is assumed to be constant and equal to 1.4. The perfect-gas state equation reads under this normalization:

$$\gamma M^2_\infty p = \rho T.$$

The dynamic viscosity μ obeys Sutherland's law:

$$\mu(T) = T^{\frac{3}{2}} \left(\frac{1+S}{T+S} \right), \quad S = 110.4K/T_\infty.$$

The free-stream Mach number is 2.5. The Reynolds number based on the free-stream velocity and the inlet boundary-layer thickness is fixed to 9600. The computational domain length in the streamwise (x) direction is $14.8\delta^i_{99}$ and in the spanwise direction (z) is $4\delta^i_{99}$. The distance between the upper plane and the adiabatic wall is $3.1\delta^i_{99}$. The flow is assumed to be periodic in the spanwise direction. Sponge regions are used at the outlet ($x \geq 14\delta^i_{99}$) and near the upper plane ($y \geq 2.5\delta^i_{99}$). The downstream recycling station is located at $x_r = 8.5\delta^i_{99}$. We use 512 grid points in x, 128 in y and 256 in z. In terms of wall-unit (using the friction velocity at the recycling location), the first grid point from the wall is located at $y^+ = 0.7$, $\Delta^+_x = 5.46$ and $\Delta^+_z = 2.9$. The domain size in wall-units is $L^+_x \times L^+_y \times L^+_z$=2797 $\times$ 586 $\times$ 756.

B. Inflow generation

Different approaches to simulate turbulent boundary layers, including temporal boundary layer (TDNS), extended TDNS (ETDNS) and spatial boundary layer (SDNS), have been reported in the literature. In the latter case, the simulation generates its own inflow conditions by rescaling the flowfield at a downstream

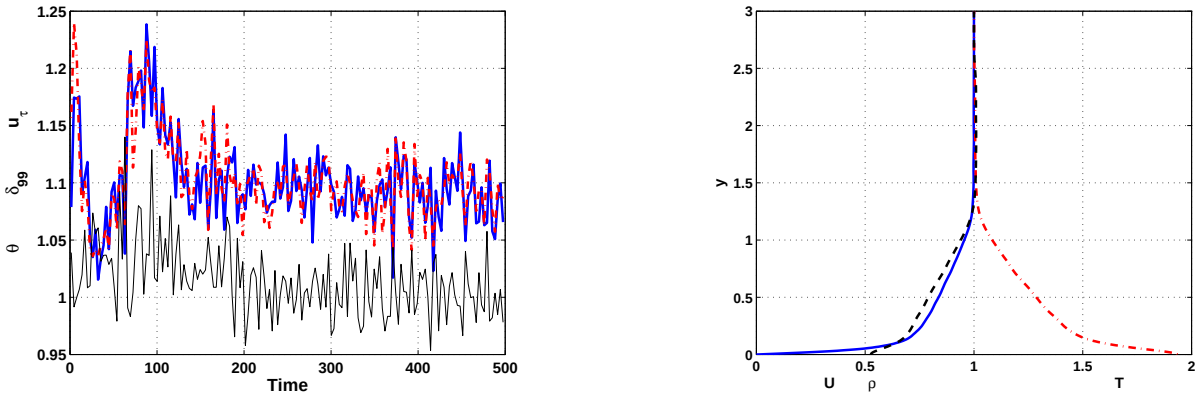

Figure 5. Left: Temporal evolution of boundary-layer thickness ratio $\frac{\delta^r_{99}}{\delta^i_{99}}$ (dashed red), friction velocity ratio (thin black) $\frac{u^i_\tau}{u^r_\tau}$ and momentum thickness (solid blue) $\frac{\theta^r}{\theta^i}$. Right: Mean-flow profiles of streamwise velocity $\overline{u}$ (solid-blue), temperature $\overline{T}$ (dash-dotted red) and density $\overline{\rho}$ (dashed-black) at the recycling station.

station and prescribing it at the inlet. This method was applied by Lund *et al.*[20] for incompressible boundary layer and its extension to the compressible flow was developed by Urbin & Knight.[19] Further development of the method was carried out, among others, by Stolz & Adams,[21] Sagaut *et al.*[23] and Xu & Martin,[22] who minimized the empirical part of the recycling by using appropriate approximations. In most these studies, the initial condition was already a turbulent state taken from another simulation. In this paper, we present a systematic method to obtain a turbulent boundary layer starting from a laminar flow field. Our procedure is outlined below.

The law-of-the-wall, well known in incompressible flow, can be extended to the compressible flow, provided that the velocity is defined by a density-weighted transformation:

$$u^{\mathrm{vd}} = \int_0^{\overline{u}} \left(\frac{\overline{\rho}}{\rho_w}\right)^{1/2} d\overline{u},$$

where u^{vd} denotes the van Driest velocity and ρ the density. The mean quantities (averaged in the spanwise direction) are denoted by an overbar while the subscript "w" refers to wall quantities, which are also averaged in the spanwise direction. The script "i" ("r") denotes quantities computed at the inlet (the recycling station). Using this velocity, the two-layer similarity laws read:

$$\frac{u^{\mathrm{vd}}(x_i, y_i^+)}{u_\tau(x_i)} = \frac{u^{\mathrm{vd}}(x_r, y_r^+)}{u_\tau(x_r)}, \tag{1}$$

$$u^{\mathrm{vd}}\left(x_i, \frac{y}{\delta^i_{99}}\right) = \left(1 - \frac{u_\tau(x_i)}{u_\tau(x_r)}\right) u^{\mathrm{vd}}_\infty + \frac{u_\tau(x_i)}{u_\tau(x_r)} u^{\mathrm{vd}}\left(x_r, \frac{y}{\delta^r_{99}}\right) \tag{2}$$

where u^{vd}_∞ is the transformed free-stream velocity and u_τ is the friction velocity $u_\tau = \sqrt{\frac{\tau_w}{\rho_w}}$, with the wall shear stress $\tau_w = \mu_w \left(\frac{d\overline{u}}{dy}\right)_{y=0}$. Then, the mean flow at the inlet $\overline{u}_i$ is obtained by using a smooth blending between the two layers, using a suitable function (see e.g. Ref.[20]). For the wall-normal velocity profile, we assume that a scaling similar to the one described above can be applied, whereas the mean profile for the spanwise velocity is zero. The mean temperature profile is derived using the Crocco-Busemann approximation across the entire boundary layer:

$$\frac{\overline{T}_i}{T_\infty} = \frac{T_w}{T_\infty} - r\frac{\gamma - 1}{2} M^2_\infty \left(\frac{\overline{u}_i}{U_\infty}\right)^2, \quad r = 0.82$$

Then, using the perfect-gas law, the mean density profile can be deduced since the pressure is nearly constant

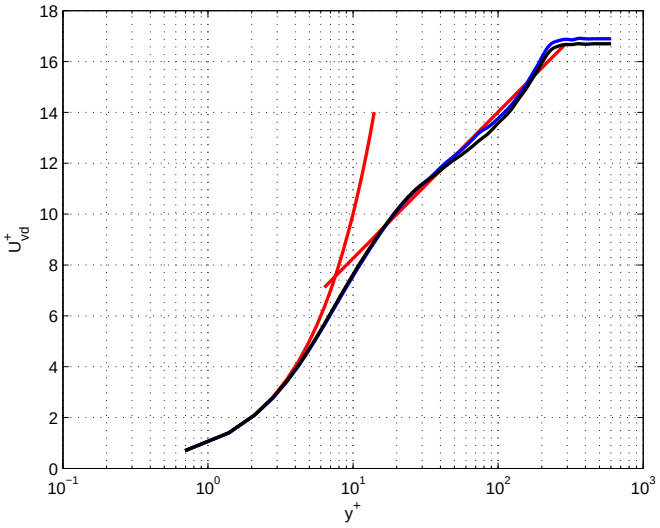

Figure 6. Van Driest transformed mean-velocity profile $u_{\rm vd}$ in wall-units y^+. Left (resp. right) quantity in Eq. 4 in black (resp. blue) line. In solid red lines, the laws of the wall $u^+ = y^+$ and $u^+ = 1/(0.4)\ln(y^+) + 2.5$.

through the boundary layer:

$$\frac{\overline{\rho}_i}{\rho_\infty} = \frac{T_\infty}{\overline{\overline{T}}_i}.$$

The perturbations, denoted with a prime and computed by subtracting the mean value from the flow field, can be assumed to satisfy a similarity law across the boundary layer. Therefore, they are rescaled and introduced at the inlet according to:

$$u'_i(y) = u'_r(\frac{\delta^r_{99}}{\delta^i_{99}}y), \tag{3}$$

where u' represents the streamwise velocity perturbation. The same procedure is applied to the spanwise w' and wall-normal v' perturbations. Then, by assuming that the pressure fluctuations are negligible, the density perturbation are obtained from the temperature fluctuations, which are in turn, related to u' through the strong Reynolds analogy:

$$\frac{\rho'}{\overline{\rho}_r} = -\frac{T'}{\overline{\overline{T}}_r}, \quad \frac{T'}{\overline{\overline{T}}_r} = -\left(\gamma - 1\right) M^2_\infty \frac{u'}{\overline{u}_r}.$$

Note that the above assumptions do not have to be correct. For example, in Ref.,[23] the pressure fluctuations are not negligible compared to the density and temperature fluctuations.

C. Initial condition

For the initial condition, a parallel flow is prescribed using the power-law profile $u|_{t=0} \equiv u(x, y, t = 0) = min(1, y^{1/3})$. The two other velocity profiles are zero. The temperature is given by the Walz equation $\frac{T(x,y,t=0)}{T_\infty} = \frac{T_w}{T_\infty} - r\frac{\gamma-1}{2}M^2_\infty \left(\frac{u|_{t=0}}{U_\infty}\right)^2$. The initial temperature at the wall, T_w, is given by $T_w = 1 + r\frac{\gamma-1}{2}M^2_\infty$ with the recovery factor $r = 0.82$. The initial density field is obtained through the state equation: $\frac{\rho|_{t=0}}{\rho_\infty} = \frac{T_\infty}{T|_{t=0}}$. Random noise perturbations are added to these mean quantities. As they convect downstream, they are rescaled and re-introduced at the inlet. These initial disturbances grow in size and spread over the whole domain, and a stationery turbulent state is quickly reached.

D. Numerical results

Temporal evolutions of the ratios of different boundary-layer characteristics between the recycling station x_r=$8.5\delta^i_{99}$ and near the inlet x=$0.1\delta^i_{99}$ are shown in Fig. 5. Useful quantities are the boundary-layer thickness

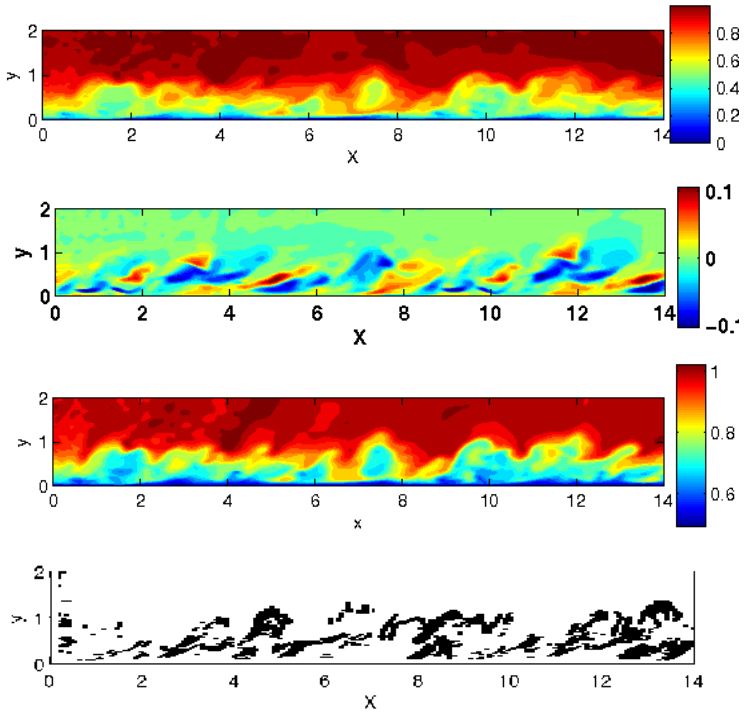

Figure 7. Top to bottom: Streamwise momentum ρu, spanwise momentum ρw, density ρ and the points where WENO is applied (depicted in black).

δ_{99}, friction velocity u_τ and the momentum thickness θ. The last quantity is computed as:

$$\theta = \int_0^\infty \frac{\overline{\rho u}}{\rho_\infty u_\infty}(1 - \frac{\overline{u}}{u_\infty})\, dy.$$

For $t \geq 140$, the flow is considered to be a stationary state since different quantities oscillate around their mean values. The temporal average of the ratio of the momentum thickness is 1.10 and of the ratio of the boundary layer thickness is 1.12. These values are in good agreement with those given by the empirical formula (see e.g. Ref.[19]):

$$\frac{\theta^r}{\theta^i} \approx \frac{\delta^r_{99}}{\delta^i_{99}} \approx (1 + \frac{x_r - x_i}{\delta^i_{99}} 0.27^{\frac{6}{5}} R_{\delta^i_{99}}^{\frac{-1}{5}})^{\frac{5}{6}}$$

and

$$\frac{u^i_\tau}{u^r_\tau} \approx (\frac{\delta^r_{99}}{\delta^i_{99}})^{\frac{1}{10}}$$

which gives the values of 1.2 and 1.01 for the ratios of the momentum thickness and friction velocity respectively. The mean value of the momentum-thickness Reynolds number $R_\theta = \rho_\infty U_\infty \theta / \mu_\infty$ is found to be around 1200. The mean temperature, density and streamwise velocity profiles are shown in Fig. 5.

Since the mean pressure is constant across the boundary layer, we have $\frac{\overline{\rho}}{\rho_w} \approx \frac{T_w}{\overline{T}}$. Therefore, the van Driest transformed streamwise velocity profile can be defined by these two equivalent forms:

$$\overline{u}^+_{\mathrm{vd}} = \int_0^{\overline{u}^+} \sqrt{\left(\frac{\overline{\rho}}{\rho_w}\right)}\, d\overline{u}^+, \quad \overline{u}^+_{\mathrm{vd}} = \int_0^{\overline{u}^+} \sqrt{\left(\frac{T_w}{\overline{T}}\right)}\, d\overline{u}^+. \tag{4}$$

These profiles are shown in Fig. 6. They are both similar and collapse with the laws of the wall. In the logarithmic region, they closely follow $(1/0.4)\ln(y^+) + 2.5$.

Finally, contours of the streamwise and spanwise velocity momentum are shown in Fig. 7. As a thermodynamic quantity, the density is considered and its contours are also shown. With the relatively low Mach number, the WENO scheme is used in few locations. For an illustration purpose, we have decreased the

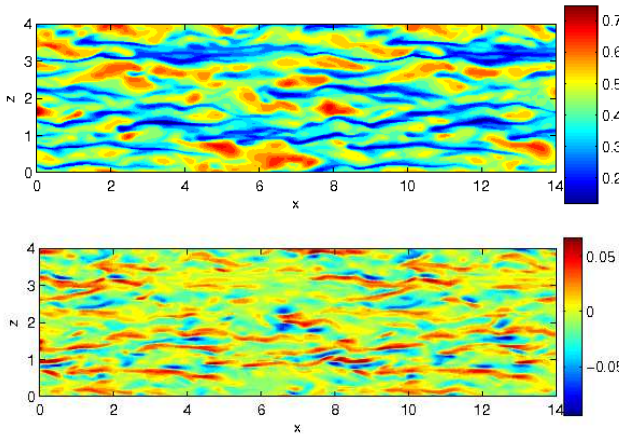

Figure 8. Streamwise (top) and wall-normal (bottom) momentum for $y^+ = 20$ ($y = 0.1$).

threshold above which the flow is considered as non-smooth. Doing so, WENO is being applied in much more points, as shown in Fig. 7 An instantaneous picture of the streamwise and wall-normal momentum at $y^+ = 20$ is shown in Fig. 8. Streamwise elongated structures are clearly evident, reminiscent of near-wall turbulence structures in incompressible turbulent boundary layers.

VI. Conclusion and Future Work

In this paper, we first examined the capability of a hybrid method in computing the shock wave-boundary layer interactions. The method conjugates the computational efficiency of a 4th-order finite difference scheme with the shock capturing ability of a 5th-order WENO scheme. The presented results show many features in close agreement with the results in the literature, hence supporting our numerical approach. Then, we have simulated a spatially developing boundary layer at Mach number 2.5 and a momentum-thickness based Reynolds number $R_\theta \approx 1200$. This boundary layer generates its own inflow by rescaling and re-introducing the flow-field from a downstream location. Beyond the presented preliminary results, the study of the influence of the domain size (and the resolution) on the mean profiles and the turbulence structures and statistics is our next step. Regarding the rescaling method, it requires further improvements, and this will be the subject of our future work.

As for the numerical approach, it is quite simple and efficient. Without any optimization, this hybrid algorithm is nearly three times faster than a standard WENO scheme. For higher Reynolds numbers, higher order hybrid methods could be needed. Modified finite difference or compact schemes, where the coefficients are chosen to increase the range of resolved wavenumbers, can also be applied instead of the usual finite difference scheme (e.g. Hill & Pullin[18]). However, the time efficiency of the method may be degraded due to the matrix inversion.

Acknowledgments

This work is supported by the NASA Grant/Cooperative Agreement NNX08AB39A (Program Monitor, Dr. Alan Wray of NASA Ames Research Center).

References

[1]Daru V. & Tenaud C. "Evaluation of TVD high resolution schemes for unsteady viscous shocked flows," Computers & Fluids **30** 89–113, 2001.

[2]Shu C.-W.& Osher S., "Efficient implementation of essentially non-oscillatory shock-capturing schemes," J. Comp. Phys. **83**, 1989.

[3]Jiang G.S. & Shu. C.W. "Efficient implementation of weighted ENO schemes," J. Comp. Phys. **126** (1) 202–228, 1996.

[4]Weirs V.G. & Candler G.V., "Optimization of weighted ENO schemes for DNS of compressible turbulence," Technical

Paper 97-1940 (AIAA Press, Washington, DC) 1997.

[5]Martn, M.P. Taylor E.M, Wu M, Weirs V.G. "A bandwidth-optimized WENO scheme for the effective direct numerical simulation of compressible turbulence." J. Comp. Phys. **220** 270–289, 2006.

[6]Wang Z.I. & Chen R.F. "Optimized weighted essentially nonoscillatory schemes for linear waves with discontinuity." J. Comp. Phys. **174** 381–404, 2001.

[7]Adams N.A. & Shariff K. "A high-resolution hybrid compact-ENO scheme for shock-turbulence interaction problems." J. Comp. Phys. **127** (1) 27–51, 1996.

[8]Adams N. "Direct numerical simulation of turbulent compression ramp flow," Theor. Comput. Fluid Dynamics, **12**, 109–129, 1998.

[9]Adams N. "Direct simulation of turbulent boundary layer along a compression ramp, at M=3 and Re=1685," J. Fluid Mech., **420**, 47–83, 2000.

[10]Pirozzoli S. "Conservative hybrid compact-WENO schemes for shock-turbulence interaction," J. Comp. Phys. **178**, 81–117, 2002.

[11]Ren Y.-X.,Liu M. & Zhang H. "A characteristic-wise hybrid compact-WENO scheme for solving hyperbolic conservation laws" J. Comp. Phys. **192**, (2), 365–386, 2003.

[12]Kim D.& Kwon J.H. "A high-order accurate hybrid scheme using a central flux scheme and a WENO scheme for compressible flow field analysis," J. Comp. Phys. **210** (2) 554–583, 2005.

[13]Van Wie D.M., Drewry Jr. D.G., King D.E., & Hudson C.M. "The hypersonic environment: Required operating conditions and design challenges," J. Mat. Science. **39** (19), 5915–5924, 2004.

[14]Weber Y.S., Oran E.S., Boris J.P., & Anderson, Jr J.D. "The numerical simulation of shock bifurcation near the end wall of a shock tube," Phys. Fluids **7**, 2475, 1995.

[15]Davies L. & Wilson J.L., "Influence of reflected shock and boundary-layer interaction on shock-tube flows," Phys. Fluids **12**, 1–37, 1969.

[16]Sjogreen B.& H.C. Yee H.C., "Grid convergence of high order methods for multiscale complex unsteady viscous compressible flows," J. Comp. Phys. **185** 1–26, 2003.

[17]Dubroca. B. "Positively conservative Roe's matrix for Euler equations," Lecture notes in physics, **515** 272–277, 1998.

[18]Hill D. & Pullin D., "Hybrid tuned center-difference-WENO method for large eddy simulations in the presence of strong shocks," J. Comp. Phys. **194**, 435–450, 2004.

[19]Urbin G. & Knight D. Large-Eddy Simulation of a spuersonic boundary layer using an unstructured grid. AIAA J. Vol **39**, (7), (2001), 1288–1295.

[20]Lund T. Wu, X. & Squires K. Generation of turbulent inflow data for spatially developing boundary layer. J. Comp. Phy. **140**, (2), (1998), 233–258.

[21]Stolz S. & Adams N.A. Large-eddy simulation of high-Reynolds-number supersonic boundary layers using the approximate deconvolution model and a rescaling and recycling technique. Phys. Fluids, **15**, (8), (2003), 2398–2412.

[22]Xu S. & Martin P. Assessment of inflow boundary conditions for compressible turbulent boundary layers. Phys. Fluids, **16**, (7), (2004), 2623–2639.

[23]Sagaut P., Garnier E., Tromeur E., Larcheveque L., Labourasse E., Turbulent inflow conditions for large-eddy simulation of compressible wall-bounded flows. AIAA J., **42**, (3), (2004), 469–477.